Four-Leg Soft-Switched Active Rectifier for Non-Isolated EV Chargers

Manfredi Gangi
Dept. of Electrical Engineering
Columbia University
New York, NY USA
manfredi.gangi@columbia.edu

Matthias Preindl
Dept. of Electrical Engineering
Columbia University
New York, NY USA
matthias.preindl@columbia.edu

Abstract—A four-leg active rectifier that could be implemented as a grid interface power-factor correcting (PFC) component of a two-stage non-isolated on-board electric vehicle (EV) charger is proposed in this paper. The analyzed converter leverages existing three-phase topology by extending it to work also in a four-wire configuration, allowing to control the current in the neutral conductor. The control algorithm is performed in a $dq\delta\sigma$ reference frame, which is generated through the introduction of a modified Clarke-Park transformation that exploits the differential and common mode signal decomposition to decouple the neutral current control and the regulation of the common mode voltage. Moreover, a discrete Variable Frequency Critical Soft Switching (VFCSS) technique is used to increase the efficiency of the converter by maintaining soft-switching operation. The proposed topology and control scheme are verified through a simulated model in PLECS. Simulation results have been reported for both balanced and unbalanced three-phase scenarios, showing that the fourth leg can be controlled to generate different current set-points in order to adapt to the three-phase currents.

Index Terms—Transformerless EV Charger, Non-Isolated Chargers, Four-Leg Converter, Power Electronics

I. INTRODUCTION

In recent years, the adoption of electric vehicles (EVs) has significantly risen, now accounting for a significant portion of total car sales. Indeed, in 2023 it has been reported that EVs share were the 18% of the total car sales, 4% more respect to 2022 [1]. Given this huge increment in the usage of electric cars, it is of paramount importance to perform further investigation regarding the development of the charging infrastructure, both on-board and off-board the vehicle, as cost and charging time remain significant barriers to foster EV penetration. Depending on the type of charging mode, EV batteries can be charged either using an external power converter directly connected to the battery, namely the off-board charger, or through the interaction of the ac mains and a converter installed inside the vehicle, which is called the on-board charger. Specifically, off-board standalone chargers are used for Level 3 fast charging applications (30 kW-360 kW), while on-board devices are designed for Level 2 power ratings (3 kW-22 kW) in order to limit the size of the components [2]. Indeed, fast charging power stations are only installed in public locations, which makes Level 2 charging more accessible since it is possible to achieve the aforementioned power ratings in more areas, such as private housing and workplace environ-

ments [3]. For this reasons, it is fundamental to investigate new possible configurations for on-board chargers which could lead to more efficient devices in terms of power density, cost and size.

The general structure of an on-board EV charger usually includes two stages: a grid side AC/DC rectifier, working as a power-factor correcting (PFC) stage, and a DC/DC component which interfaces the battery with the DC bus and regulates the charging operation [4]. Moreover, in literature, EV chargers are usually classified as isolated or non-isolated depending on whether or not a galvanic isolation is inserted in the topology. In [5], several isolated on-board EV charger configurations have been reviewed, highlighting new trends and challenges, such as the need for higher power chargers to match the increased batteries size, and the interoperability of a charger in different grid configurations. On the other hand, due to the absence of galvanic isolation, non-isolated chargers can achieve greater efficiencies and reduce the total costs because the converter can be easily integrated in the drivetrain of the vehicle [6]. The reason why this type of configuration has not been extensively adopted is related to the potentially large leakage current that can circulate due to the lack of high common mode (CM) impedance introduced by the isolation stage [7]. However, given also the development of transformerless inverter in the PV industry [8], recent studies started analyzing the benefits of non-isolated chargers adopting different configurations and control techniques to solve the leakage current problem. [9], [10] and [11] analyzed transformerless charger structures with three-phase grid interface, employing control and filtering techniques to mitigate leakage current. A different approach is shown in [12], where symmetrical modulation is used in a single-phase charging application to block leakage current circulation. These studies have achieved excellent results in mitigating leakage current to be compliant with the automotive standards, however there is still room for improvement since new topologies can be introduced to achieve a multi-grid interface, and a better independent control of the three-phase voltages, especially in unbalanced operating conditions.

In this view, this paper aims to contribute to the research on transformerless charger, proposing a non-isolated soft-switched active rectifier with the advantage of being re-
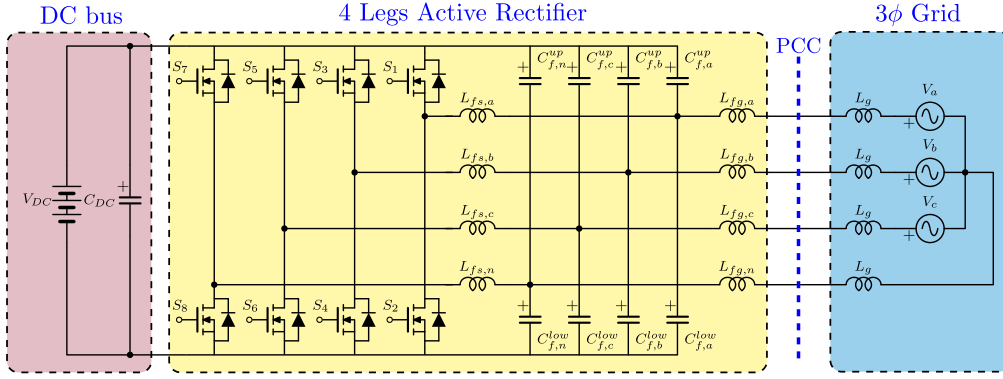
Fig. 1. Four-Leg Active Rectifier with 3ϕ grid interface.

configured to accommodate both single and three-phase grid configurations, adding a fourth leg to control the neutral current. Four wire configurations for the PFC stage of the three-phase charger have been described in [13] and [14], demonstrating that adding a fourth leg reduces the CM noise and improves the overall efficiency of the converter. This analysis focuses on leveraging the general topology described in [9] introducing a fourth leg for the neutral conductor and using an extended Clarke-Park transformation and a Variable Frequency Critical Soft Switching (VFCSS) technique (accurately described in [15]) to control the converter.

The paper is organized as follows: Section II introduces the proposed topology of the power converter, along with its control scheme for the three-phase grid interface. Section III presents the results obtained from the simulated model. To conclude, Section IV reports the final considerations.

II. TOPOLOGY AND CONTROL

The proposed four-leg active rectifier topology consists of four half-bridges, one for each phase, and it is shown in Fig. 1. As shown in [9], the most notable difference of the proposed configuration with respect to typical grid-tied inverter topology is represented by the filtering capacitors, which usually have their star point floating or, in four wire configurations, connected to the neutral conductor [16]. In the analyzed topology, the filtering capacitors are split into two equal upper and lower capacitors, which are then respectively connected to the positive and negative DC link. The advantages of these modifications are mainly two. Connecting all the capacitors back to the switches allows to control the common-mode voltage of these capacitors, decreasing leakage current circulation, which is one of the main issues related to the adoption of non-isolated EV chargers. Secondly, inserting a lower and an upper capacitor helps reducing ripple currents, decreasing overall capacitance and improving conducted EMI [17].

Another significant benefit of the proposed circuit configuration is being modular. Each leg displays the same configuration both in terms of switches and filters, making it possible to re-configure the device also for single-phase applications by connecting together the first two phases to form the positive terminal and the other two to create the neutral as it is shown in Fig. 2. The presence of the fourth leg connected to the neutral conductor allows to control also the current flowing through that wire, making the proposed active rectifier suitable for unbalanced scenarios. In the following, it is presented the control scheme used for this converter, where a modified version of the Clarke and Park transformations are introduced.

A. Control AC/DC

The proposed converter is controlled in a synchronous reference frame through the introduction of a modified Clarke-Park transformation. Compared to the standard transformations described in [18] and their extension for four phase systems [19], the considered mathematical operation keeps the nature of the standard three-phase system while considering also the neutral conductor. Specifically, the canonical amplitude-invariant Clarke transformation is modified by adding an extra component V_z which represents the neutral voltage without any scaling factor.

The extended Clarke transformation used is

$$\begin{bmatrix} V_\alpha \\ V_\beta \\ V_0 \\ V_z \end{bmatrix} = \frac{2}{3} \begin{bmatrix} 1 & -\frac{1}{2} & -\frac{1}{2} & 0 \\ 0 & \frac{\sqrt{3}}{2} & -\frac{\sqrt{3}}{2} & 0 \\ \frac{1}{2} & \frac{1}{2} & \frac{1}{2} & 0 \\ 0 & 0 & 0 & \frac{3}{2} \end{bmatrix} \begin{bmatrix} V_A \\ V_B \\ V_C \\ V_N \end{bmatrix} \tag{1}$$

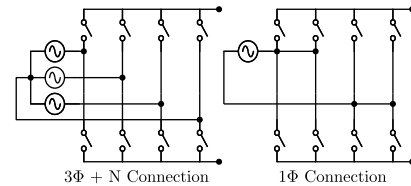$$= \boldsymbol{A_{\alpha\beta0z}} \begin{bmatrix} V_A \\ V_B \\ V_C \\ V_N \end{bmatrix}$$

Fig. 2. Grid-side connection of the proposed active rectifier for three-phase and single-phase grids.

where V_A, V_B, V_C and V_N are the voltages of the lower filtering capacitors measured with respect to the negative DC link.

The second modified operation is the Park transformation, where the usual zero-sequence component is split into two variables. The proposed version is the following

$$\begin{bmatrix} V_d \\ V_q \\ V_\delta \\ V_\sigma \end{bmatrix} = \begin{bmatrix} \cos\theta & \sin\theta & 0 & 0 \\ -\sin\theta & \cos\theta & 0 & 0 \\ 0 & 0 & \frac{1}{2} & -\frac{1}{2} \\ 0 & 0 & \frac{1}{2} & \frac{1}{2} \end{bmatrix} \begin{bmatrix} V_\alpha \\ V_\beta \\ V_0 \\ V_z \end{bmatrix} \tag{2}$$

$$= \boldsymbol{A_{dq\delta\sigma}} \begin{bmatrix} V_\alpha \\ V_\beta \\ V_0 \\ V_z \end{bmatrix} = \boldsymbol{A_{dq\delta\sigma}} \boldsymbol{A_{\alpha\beta0z}} \begin{bmatrix} V_A \\ V_B \\ V_C \\ V_N \end{bmatrix}$$

where, due to the presence of V_0 and V_z derived from the extended Clarke, two new variables are introduced. Specifically, V_δ considers the difference between the three-phase average voltage and the neutral voltage, while V_σ represents the sum of the three-phase average voltage and the neutral voltage. This transformation derives from the common and differential mode signal decomposition and can be explained graphically in Fig. 3, where the I_δ component will be generated by a difference between the three-phase zero sequence voltage (V_0) and the neutral voltage (V_z), giving the possibility to control the current flowing through the neutral, while the I_σ term represents the control of the common-mode voltage of the four legs, working as the canonical zero-sequence control. Indeed, the same transformations are also applied for the measured currents as described in the following description of the control algorithm.

Having defined this modified Clarke-Park transformation, the control of the converter is performed in the $dq\delta\sigma$ domain using Proportional Integral (PI) regulators. Fig. 4 shows an high-level diagram of the control algorithm used for this active rectifier where each green block represents a PI component. Moreover, some assumptions have been introduced regarding the controlling of the device. Firstly, the grid-side filter inductor and the grid inductance are merged together into one lumped component L_g inserted on the grid side. Secondly, the "DC bus Control" and the "Reactive Power Control" shown in Fig. 4 are neglected in this study, since the references for the grid d and q currents are manually generated.

Focusing on the different control loops, the grid d-current is controlled in order to keep the DC bus voltage stable while an hypothetical second stage DC/DC converter, which operates at the battery interface, regulates the charging and discharging of the battery. Indeed, as previously stated, in this analysis the current will be controlled to follow a fixed reference to simulate constant active power transferring. Then, grid q-current reference is set to zero since no reactive power transfer is analyzed. However, it could be generated depending on the reactive power controller to perform grid services operations as in [10]. Moving to the third loop, the grid δ-current control block manages the current flowing through the
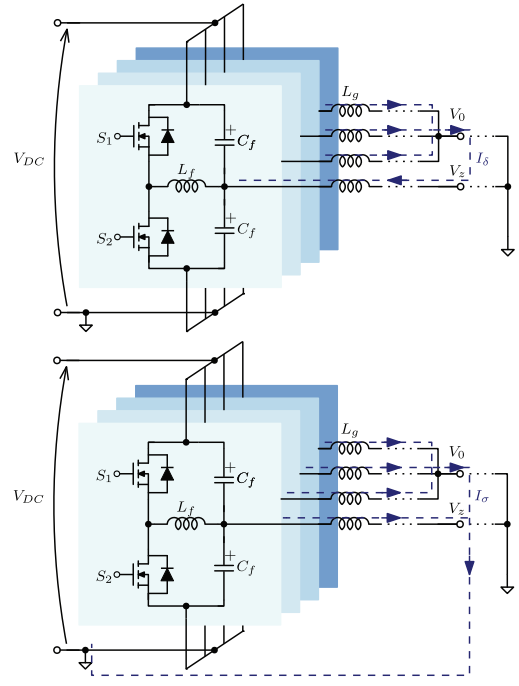

Fig. 3. Differential(δ) mode current decomposition introduced in the extended Park transformation (upper figure). Common(σ) mode current decomposition of the modified Park transformation (lower figure).

neutral conductor and it is set to zero to simulate a balanced three-phase scenario, but it can also be controlled to deal with unbalance conditions or applications where the neutral is used as return conductor. Lastly, the grid σ-voltage is controlled to be stable at half of the DC bus, in order to avoid leakage current flowing back to the grid since the zero sequence current will be captured by the filtering capacitors.

The proposed converter exploits the VFCSS technique, which allows to substitute high turn-on losses of the upper switch with low turn-off losses of the lower switch of the leg. This algorithm uses the switching frequency to regulate the filter inductor ripple current so that peak and valleys of the that current can be placed in order to satisfy the soft-switching boundary condition. The switching frequency is calculated with

$$f_{sw} = \frac{(1-D)DV_{DC}}{2(|I_L^{avg}| + I_L^{thr})L_f} \tag{3}$$

where D is the duty cycle, V_{DC} is the voltage at the DC link, I_L^{avg} is the average current across the filter inductor L_f and I_L^{thr} is a threshold current whose value is set depending on the soft-switching boundary conditions of the specific case. More details regarding this switching technique are described in [15] and [20].

III. SIMULATION RESULTS

The analyzed converter and its control algorithm have been validated through a simulated model using Matlab/Simulink
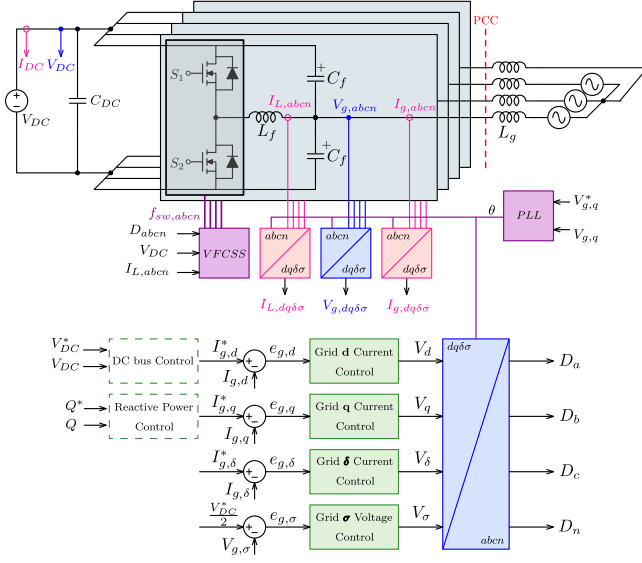
Fig. 4. High-level scheme of the control algorithm for the active rectifier.

TABLE I
MAIN PARAMETERS USED FOR THE SIMULATION IN PLECS.

Parameters	Description	Value
V_{DC}	Voltage at the DC link	800 V
V_g^{LL}	Line-to-line grid voltage	400 V
L_f	Switch side filer inductance	8 μH
$L_{f,ESR}$	Parasitic resistance of the inductor	15 mΩ
C_f	Global filter capacitance of each leg	12 μF
$C_{f,ESR}$	Parasitic resistance of the capacitor	3.5 mΩ
C_{DC}	DC bus capacitance of each leg	24 μF
L_g	Grid side inductor and grid line inductance	15 μH
$L_{g,ESR}$	Parasitic resistance of the inductor	7.5 mΩ
F_g	Grid Frequency	50 Hz
I_{RMS}	RMS Current	16 A
$I_{g,q}^*$	Grid q-current reference	0 A

and PLECS. The main parameters used for the different simulated scenarios are shown in Table I. In particular, two cases have been analyzed in order to verify the correct functionality of the power converter and the control scheme adopted. The first one shows the EV charger working in a balanced three-phase system, while the second one demonstrates the ability of the topology to work in unbalanced conditions.

A. Balanced Scenario

In this case, to simulate the regular operation of the charger in a balanced three-phase system, the d-current is set to a non-zero value, while q and δ currents are set to zero to ensure no reactive power flowing and zero current in the neutral conductor. The main results are shown in Fig. 5 and in Fig. 6. In particular, Fig. 5 depicts the switch-side inductor currents, which shows three different behaviors depending on the regulator on-state and on the d-current reference. The current trend matches with the expected theoretical one generated using the discrete VF-CSS technique since the switching frequency is higher around the zero-crossing of the signal, while it decreases approaching the crest of the waveform, as also shown in [15]. The output voltage and current at the
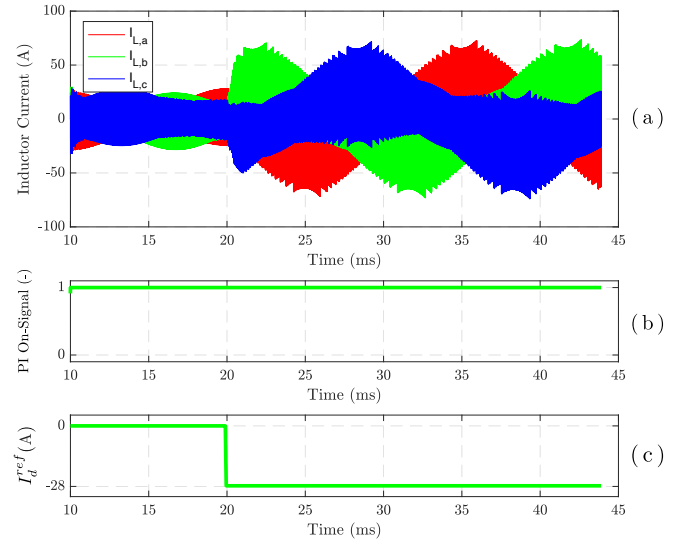

Fig. 5. (a) Currents flowing in the switch-side inductors, which shows different trends depending on the PI state and d-current reference. The interval from 0 to 10 ms is omitted since it shows the transient with no active regulators. (b) PI on-state signal, which is triggered at 10 ms. (c) Reference signal applied to the d-current controller at 20 ms.

point of common coupling (PCC) are displayed in Fig. 6. Specifically, in Fig. 6 -(a) it can be noticed that the three-phase output voltage is controlled to be centered at $0.5V_{DC}$, matching with the neutral voltage (V_n). Fig. 6 -(b) represents the output current at the PCC where it is possible to see that, as soon as the regulators are in their active state and the current reference is set to $-\sqrt{3}I_{RMS}$, the output current tends to behave as a balance three-phase current, with the neutral current fixed at zero confirming the robustness of the model in this scenario.
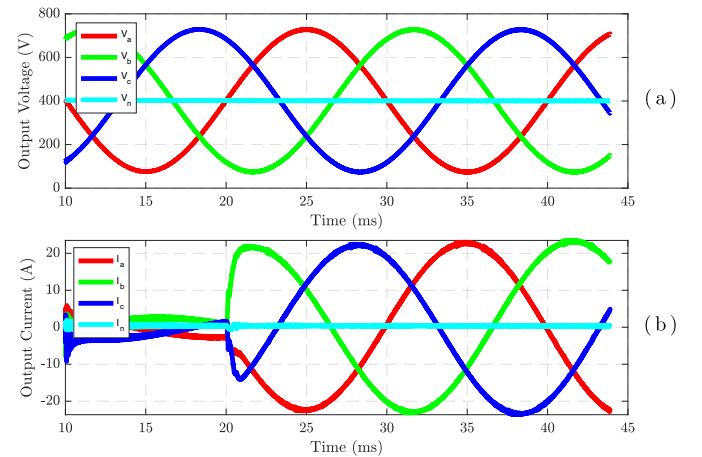

Fig. 6. (a) Output voltage measured at the PCC for a balanced three-phase system centered at $0.5V_{DC}$ (400 V). The interval from 0 to 10 ms is omitted since it shows the transient with no active regulators. (b) Output current measured at the PCC for a balanced three-phase system with zero current flowing through the neutral wire. The interval from 0 to 10 ms is omitted since it shows the transient with no active regulators.

B. Unbalanced Scenario

This scenario describes the case during which the sum of the three-phase currents is different from zero, generating a fourth current flowing through the neutral conductor since

$$i_a + i_b + i_c + i_n = 0. \tag{4}$$

The goal of this simulation is to highlight the fact that, by exploiting the δ-current controller, it is possible to set up whichever type of current in the neutral wire, making the EV charger capable of operating also in unbalanced scenarios.

The new reference signals for this operating mode are the same described in the aforementioned balanced scenario, except for the δ-current, whose value is set to 20 A after 40 ms as shown in Fig. 7 -(c). In this case, as shown in Fig. 7 -(a), the currents flowing through the switch-side inductors will depict a different behaviour after the step applied to the δ-current reference signal since the fourth leg will generate a negative current to mitigate the positive increment of the average of the three-phase currents. In Fig. 8 -(b) it is possible to see the output currents measured at the PCC, which behave in accordance with the switch-side inductor currents and with the linear transformations introduced in the controller. Indeed, the mathematical relation between the controlled currents is

$$I_\delta = \frac{I_0 - I_z}{2} \tag{5}$$

where I_0 is the average of the three-phase currents and I_z is equal to the current crossing the neutral wire (I_n). The output currents measured and shown in Fig. 8 -(b) are consistent with the aforementioned condition, ensuring the correct functioning of the control algorithm. Regarding the output voltages, the behaviour is the same as in the previous scenario, where the
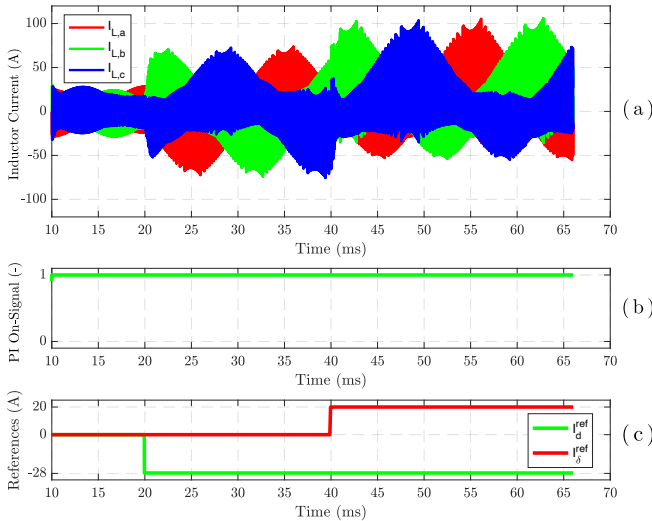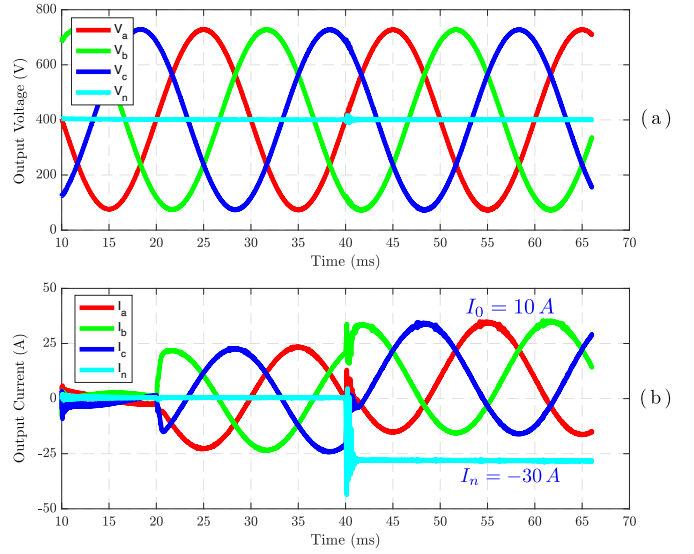

Fig. 8. (a) Output voltage measured at the PCC for the unbalanced current scenario. The interval from 0 to 10 ms is omitted since it shows the transient with no active regulators. (b) Output current measured at the PCC showing the transition from balanced to unbalanced operating conditions. The interval from 0 to 10 ms is omitted since it shows the transient with no active regulators.

average voltage is set at $0.5 V_{DC}$ and overlaps with the neutral voltage.

In this case, the δ-current reference is set to a constant value. However, apart from physical limits related to the maximum achievable current and power, the fourth leg can follow various types of signals, enabling the opportunity of using the EV charger also for Vehicle-to-Everything(V2X) applications where unbalanced loads are supplied.

IV. CONCLUSIONS

This paper analyzed a novel four-leg soft-switched active rectifier which could be used as an AC/DC conversion unit for a non-isolated onboard EV charger. The proposed configuration aims at controlling each phase voltage independently, regulating also the neutral current. The charger is controlled using a modified Clarke-Park transformation, which exploits the differential and common mode signal decomposition to decouple the neutral current control and the regulation of the common mode voltage, which is stabilized at $0.5 V_{DC}$ to block leakage current circulation. Then, a VF-CSS scheme is applied to ensure soft-switching and reducing the overall losses of the system. The topology and the control algorithm have been validated through a simulated model in PLECS. In particular, two scenarios have been reported: a balanced three-phase operating case, where it has been demonstrated the functioning of the converter in normal operating conditions, and an unbalanced case, during which the fourth leg is controlled to generate a current to mitigate the non-zero centered three-phase currents. Indeed, the proposed converter shows the potential of being adopted for V2X applications and in different grid configurations due to its topology and control scheme.

Fig. 7. (a) Currents flowing in the switch-side inductor, which shows three different trends depending on the PI state and d-current reference. The interval from 0 to 10 ms is omitted since it shows the transient with no active regulators. (b) PI on-state signal, which is triggered at 10 ms. (c) Reference signal applied to the d-current controller at 20 ms and to the δ-current controller at 40 ms.

REFERENCES

[1] IEA, "Global EV Outlook 2023," Tech. Rep. [Online]. Available: https://www.iea.org/reports/global-ev-outlook-2023

[2] EVESCO, "Levels of charging." [Online]. Available: https://www.power-sonic.com/blog/levels-of-ev-charging/

[3] U. D. of Transportation, "Charger types and speeds," https://www.transportation.gov/rural/ev/toolkit/ev-basics/charging-speeds: :text=Level

[4] S. Rivera, S. M. Goetz, S. Kouro, P. W. Lehn, M. Pathmanathan, P. Bauer, and R. A. Mastromauro, "Charging infrastructure and grid integration for electromobility," *Proceedings of the IEEE*, vol. 111, no. 4, pp. 371–396, 2022.

[5] H. Wouters and W. Martinez, "Bidirectional Onboard Chargers for Electric Vehicles: State-of-the-Art and Future Trends," *IEEE Transactions on Power Electronics*, vol. 39, no. 1, pp. 693–716, Jan. 2024. [Online]. Available: https://ieeexplore.ieee.org/document/10265141/

[6] J. Wang, Y. Zhang, M. Elshaer, W. Perdikakis, C. Yao, K. Zou, Z. Xu, and C. Chen, "Nonisolated Electric Vehicle Chargers: Their Current Status and Future Challenges," *IEEE Electrification Magazine*, vol. 9, no. 2, pp. 23–33, Jun. 2021. [Online]. Available: https://ieeexplore.ieee.org/document/9447274/

[7] C. Stutz, S. Nielebock, and M. März, "Analytic calculation of touch and leakage currents of non-isolated ev chargers using a fast common mode calculation method and non-ideal passive component models," in *2022 24th European Conference on Power Electronics and Applications (EPE'22 ECCE Europe)*. IEEE, 2022, pp. 1–11.

[8] Y. Tang, W. Yao, P. C. Loh, and F. Blaabjerg, "Highly reliable transformerless photovoltaic inverters with leakage current and pulsating power elimination," *IEEE Transactions on Industrial Electronics*, vol. 63, no. 2, pp. 1016–1026, 2015.

[9] L. Zhou, M. Jahnes, M. Eull, W. Wang, G. Cen, and M. Preindl, "Robust Control Design for Ride-Through/Trip of Transformerless Onboard Bidirectional EV Charger With Variable-Frequency Critical-Soft-Switching," *IEEE Transactions on Industry Applications*, vol. 58, no. 4, pp. 4825–4837, Jul. 2022. [Online]. Available: https://ieeexplore.ieee.org/document/9750904/

[10] L. Zhou, M. Jahnes, M. Eull, W. Wang, and M. Preindl, "Control Design of a 99% Efficiency Transformerless EV Charger Providing Standardized Grid Services," *IEEE Transactions on Power Electronics*, vol. 37, no. 4, pp. 4022–4038, Apr. 2022. [Online]. Available: https://ieeexplore.ieee.org/document/9601271/

[11] D. Zhang, J. Kaufmann, J. Huber, M. Kasper, G. Deboy, and J. W. Kolar, "Non-isolated bidirectional three-phase three-level wide-output-voltage-range voltage dc-link ev charger," *IEEE Transactions on Transportation Electrification*, 2024.

[12] C. Viana, S. Semsar, M. Pathmanathan, and P. W. Lehn, "Integrated Transformerless EV Charger With Symmetrical Modulation," *IEEE Transactions on Industrial Electronics*, vol. 69, no. 12, pp. 12 506–12 516, Dec. 2022. [Online]. Available: https://ieeexplore.ieee.org/document/9617136/

[13] B. Strothmann, F. Schafmeister, and J. Böcker, "Common-mode-free bidirectional three-phase pfc-rectifier for non-isolated ev charger," in *2021 IEEE Applied Power Electronics Conference and Exposition (APEC)*. IEEE, 2021, pp. 2783–2790.

[14] R. Chen, J. Niu, H. Gui, Z. Zhang, F. Wang, L. M. Tolbert, B. J. Blalock, D. J. Costinett, and B. B. Choi, "Investigation of fourth-leg for common-mode noise reduction in three-level neutral point clamped inverter fed motor drive," in *2019 IEEE Applied Power Electronics Conference and Exposition (APEC)*. IEEE, 2019, pp. 2582–2588.

[15] L. Zhou and M. Preindl, "Variable Switching Frequency Techniques for Power Converters: Review and Future Trends," *IEEE Transactions on Power Electronics*, vol. 38, no. 12, pp. 15 603–15 619, Dec. 2023. [Online]. Available: https://ieeexplore.ieee.org/document/10255326/

[16] F. Rojas, R. Cardenas, C. Burgos-Mellado, E. Espina, J. Pereda, C. Pineda, D. Arancibia, and M. Diaz, "An Overview of Four-Leg Converters: Topologies, Modulations, Control and Applications," *IEEE Access*, vol. 10, pp. 61 277–61 325, 2022. [Online]. Available: https://ieeexplore.ieee.org/document/9791418/

[17] M. Jahnes and M. Preindl, "Novel Upper Capacitor for Half-Bridge Switching Converter Topologies that Reduces EMI and Capacitor Ripple Current," in *2022 IEEE Transportation Electrification Conference & Expo (ITEC)*. Anaheim, CA, USA: IEEE, Jun. 2022, pp. 37–42. [Online]. Available: https://ieeexplore.ieee.org/document/9813856/

[18] C. J. O'Rourke, M. M. Qasim, M. R. Overlin, and J. L. Kirtley, "A geometric interpretation of reference frames and transformations: dq0, clarke, and park," *IEEE Transactions on Energy Conversion*, vol. 34, no. 4, pp. 2070–2083, 2019.

[19] F. Della Torre, S. Leva, and A. Paolo Morando, "Symmetrical and clarke-park transformations for four-phase systems," *COMPEL-The international journal for computation and mathematics in electrical and electronic engineering*, vol. 27, no. 6, pp. 1370–1386, 2008.

[20] M. Jahnes, L. Zhou, Y. Fahmy, and M. Preindl, "A Peak 1.2MHz, >99.5% Efficiency, and >10kW/L Power Density Soft-Switched Inverter for EV Fast Charging Applications," *IEEE Transactions on Transportation Electrification*, pp. 1–1, 2024. [Online]. Available: https://ieeexplore.ieee.org/document/10314526/